Optics Communications 285 (2012) 546–552

Contents lists available at SciVerse ScienceDirect

Optics Communications

journal homepage: www.elsevier.com/locate/optcom

Improvement of the signal-to-noise ratio in interferometry using multi-frame high-dynamic-range and normalization algorithms

René Restrepo *, Néstor Uribe-Patarroyo, Tomás Belenguer

Laboratorio Nacional de Instrumentación Espacial (LINES), Instituto Nacional de Técnica Aeroespacial (INTA), Ctra. Ajalvir km 4, Torrejón de Ardoz, E-28850 Madrid, Spain

ARTICLE INFO

Article history:
Received 20 June 2011
Received in revised form 7 September 2011
Accepted 25 October 2011
Available online 12 November 2011

Keywords:
High dynamic range (HDR)
Normalization
Fringe analysis
Liquid crystals (LC)

ABSTRACT

Using both high dynamic range (HDR) and normalization methodologies, we show a method to improve the fringe pattern contrast in interferometric measurements normally used for phase recovering. In a simulated interferogram that mimics the main effects that can be found in an interferometric process (stray-light, photon noise, electronic noise, scattering phenomena, etc.) it was possible to improve the contrast of the fringes and to decrease the root mean square error by more than 35%. The method proposed is applied to experimental interferograms to measure wavefront error and retardance changes on liquid crystal (LC) devices. It is done by using a Mach–Zehnder set-up in which we used different polarization areas. The proposed method increases the quality of the phase recovered and decreases the root mean square error by 50%.

1. Introduction

A limited dynamic range can be a problem, and increasing it is a strong tool in many interferometric applications [1–6] or in other science areas such as computer vision [7,8] or astronomy [9], although, increasing the dynamic range is done through software, it cannot be done without CCD knowledge.

The most common CCD characterization parameters are spectral response, minimum and maximum signals, dynamic range, pixel-to-pixel uniformity, output conversion gain, noise floor, charge transfer efficiency, spectral quantum efficiency and signal-to-noise ratio [10]. As the parameters mentioned above are interdependent, if the dynamic range is extended, signal-to-noise ratio improves.

The response function or characteristic curve is the slope of the output–input transformation. The maximum input or the saturation equivalent exposure is the input that fills the charge wells. The saturation equivalent exposure is used to define the dynamic range [10]. The response function depends on the light source characteristics and the spectral quantum efficiency. The spectral quantum efficiency varies by device.

In the case of film photography, the film response to variations in exposure is a non-linear function, which is the product of the irradiance the film receives and the exposure time. The CCD sensors are designed to produce electrical signals, which are linearly proportional to the sensor exposure up to some saturation level [11]. However, the CCD imaging process usually deviates from this ideal linear model [12] due to convert 12-bit output from the CCD's analog-to-digital converters to 8-bit values commonly used to store images and other error sources in the sensor. As with film, the most significant nonlinearity in the response curve is its saturation point, where any pixel with a radiance above a certain level is mapped to the same maximum image value [13].

To obtain a high dynamic range radiance image (HDR), a set of images in different exposure times can be fused into a single radiance image with wide dynamic range, but the response function of the imaging system must be computed before [14]. All methods' essential information to radiometric calibration and its response function recovery is how brightness gray-levels in one image correspond to brightness gray-levels in another one [11–16]. The algorithm developed by Debevec and Malik [13] to response function recovery and HDR radiance map construction, was used for this work due to the easiness of the implementation.

Intensity $I(x,y,t)$ could be defined as the relationship between irradiance $E(x,y)$ and exposure times $\Delta t(t)$ as film photography, where intensity is obtained in an 8 bit range (0–255 gray scale), and it is expressed as:

$$I(x,y,t) = f(E(x,y)\cdot \Delta t(t)), \tag{1}$$

where f is the response function and it is assumed to be monotonic and invertible, Eq. (1) can be written as:

$$ln\ f^{-1}(I(x,y,t)) = ln\ E(x,y) + ln\ \Delta t(t), \tag{2}$$

as exposure times $\Delta t(t)$ and intensities $I(x,y,t)$ are known, the calibration technique is only a regularization method that allows

* Corresponding author. Tel.: +34 915206622.
E-mail address: restrepogr@inta.es (R. Restrepo).

0030-4018/$ – see front matter © 2011 Elsevier B.V. All rights reserved.
doi:10.1016/j.optcom.2011.10.077

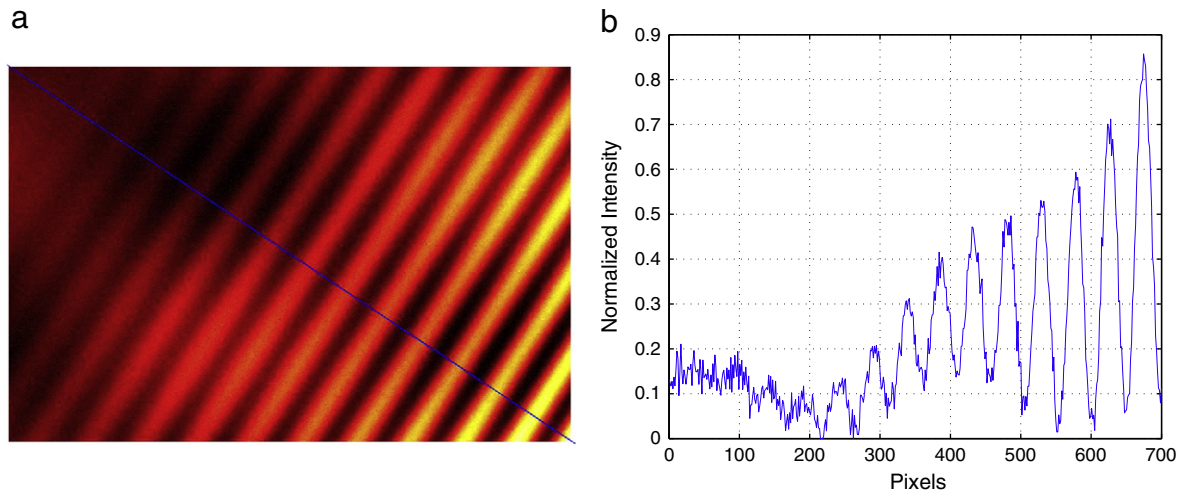

Fig. 1. The most under-saturated interferogram simulated. (a) Interferogram with 5% of noise. (b) Profile of interferogram, line on (a).

knowing the response curve of the sensor f and the irradiance $E(x,y)$; This function is solved by least square minimization.

Once the response curve is recovered, HDR can be computed in three simple steps. First, each measurement $I(x,y,t)$ is mapped to its scaled radiance value $E(x,y)$, using the recovered response function f. The response curve can be used to determine radiance values in any images acquired by the imaging process associated with f, and not only the images used to recover the response function. Second, the scaled radiance is normalized by the scaled exposure $\overline{\Delta t}(t)$ so that all radiance values end up with the same effective exposure. Finally, the radiance value at a pixel is then computed as a weighted average of its individual normalized radiance values. In the Debevec and Malik algorithm [13], the weighting function is a simple hat function based on the assumption that mid-range pixels are more reliable. However, we used the signal theory as it was proposed for Mitsunaga and Nayar [14]. Any of these methods will yield a satisfactory result, although the latter weighting function is better supported by the signal theory [16]. Eq. (2) can be rewritten to convert pixel values to relative radiance values assuming that the integration time is known.

$$ln\ E(x,y) = ln\ f^{-1}(I(x,y,t)) - ln\ \Delta t(t). \tag{3}$$

Assuming that the problem is an interferometric measurement with over-saturated and under-saturated areas, increasing the dynamic range, as mentioned before, it is not enough for a quality phase recovery. The following step would be to suppress background and to equalize modulation.

Algorithms used to visualize the HDR image [16] are not useful to HDR interferometric fringes, because they are not trivial to equalization of the modulation. However, normalization algorithms used in fringe analysis have been developed for this task [17–19]. The process of background suppression and modulation normalization is a denominated fringe pattern normalization [18]. Background and modulation variations are considered a source of phase estimation errors [17], therefore fringe normalization is a preprocess step before phase recovery. The fringe normalization algorithm used in this work was the isotropic n-dimensional fringe pattern normalization [17], developed by Quiroga et al. and it will be briefly explained.

If the fringe pattern is assumed a sinusoidal model of the irradiance can be written as:

$$I_{\mathrm{HDR}}(x,y) = b(x,y) + m(x,y)\cos\phi(x,y), \tag{4}$$

where $I_{\mathrm{HDR}}(x,y)$ is the HDR fringe pattern irradiance, $b(x,y)$ the background, $m(x,y)$ the modulation, $\phi(x,y)$ the modulating phase. $I_{\mathrm{HP}}(x,y)$

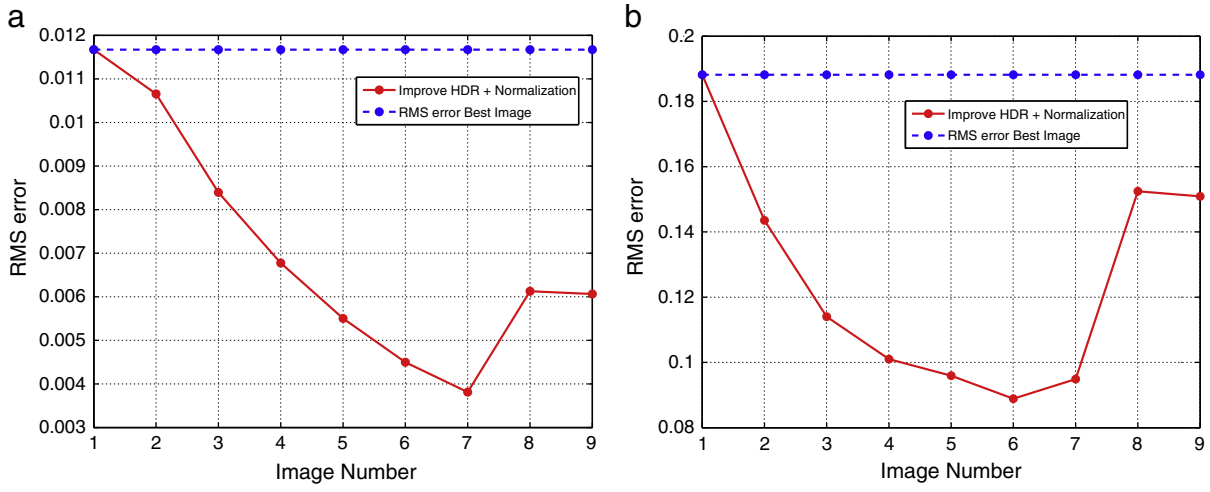

Fig. 2. Image Number vs. RMSE. (a) HDR + Normalization without noise. (b) HDR + Normalization with noise.

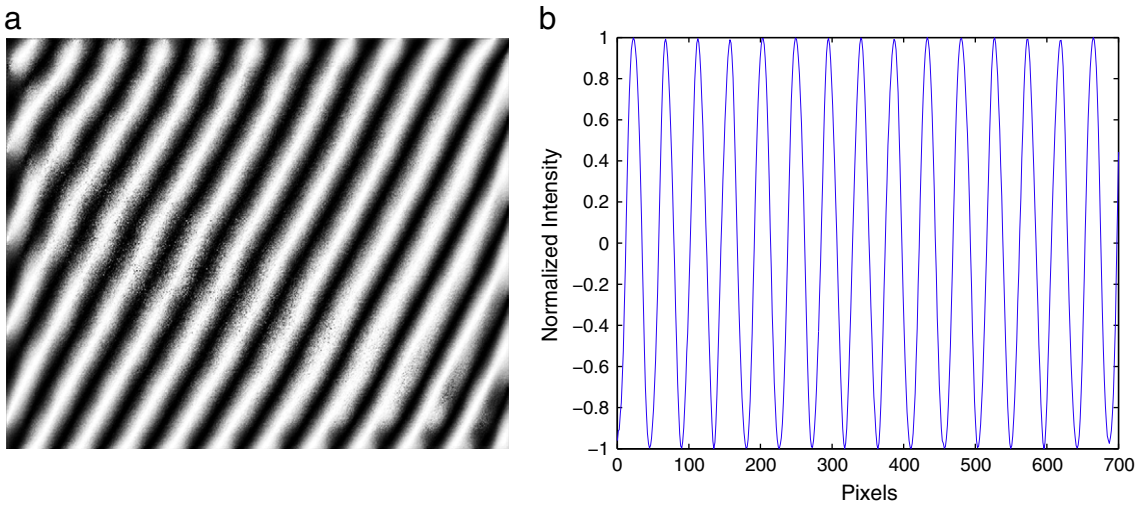

Fig. 3. Interferogram Normalized using HDR + Normalization methodology. (a) Normalized interferogram. (b) Profile of normalized interferogram.

is the HDR irradiance filtered for a high-pass filter to suppress the background. It can be written as:

$$I_{HP}(x,y) = m(x,y)\cos\phi(x,y). \tag{5}$$

After background suppression, to obtain the modulation normalization, therefore I_{HP} is normalized, and then the simple steps must be applied.

H_n is non-linear operator that can be interpreted as the n-dimensional generalization of the 1D Hilbert operator [20]. It can be computed as:

$$H_n\{I_{HP}(x,y)\} = F^{-1}\left\{-i\cdot\frac{q}{|q|}\cdot F\{I_{HP}(x,y)\}\right\}. \tag{6}$$

Eq. (6) states that the frequency response of $H_n\{.\}$ can be estimated by n 1D Reisz filters along each spectral coordinate [20]. where $q=(\mu_1,\ldots,\mu_n)$ is the position vector in the spectral domain. Then, applying the quasi-quadrature operator as it is shown:

$$\overline{Q_n}\{I_{HP}(x,y)\} = |H_n\{I_{HP}(x,y)\}|. \tag{7}$$

Finally, the fringe pattern normalized over HDR interferometric fringes is written as:

$$I_N(x,y) = \frac{I_{HP}(x,y)}{\sqrt{(I_{HP}(x,y))^2 + \left(\overline{Q_n}\{I_{HP}(x,y)\}\right)^2}}. \tag{8}$$

In summarizing, we propose a method that has two principal steps, which are to increase the dynamic range and then normalize the over HDR interferometric pattern. The main objective is o process the modulation to improve the contrast in a set of interferograms that will be used to reconstruct the phase. To demonstrate the benefit of this

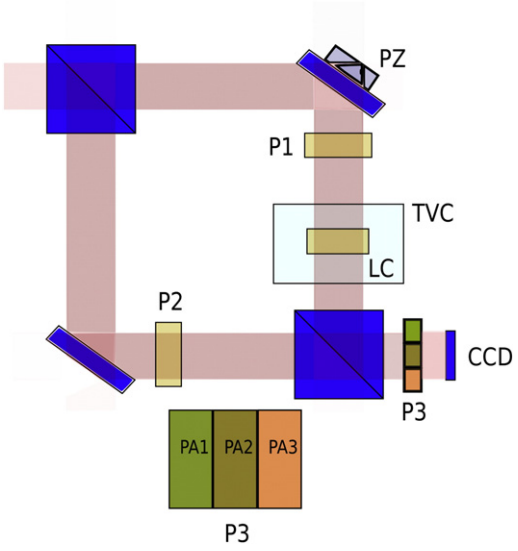

Fig. 4. Mach–Zehnder set-up. P1, P2 and P3 are polarizers. PZ piezoelectric linear stage. TVC thermo-vacuum chamber. LC liquid crystal. PA1, PA2 and PA3 Three different polarization states.

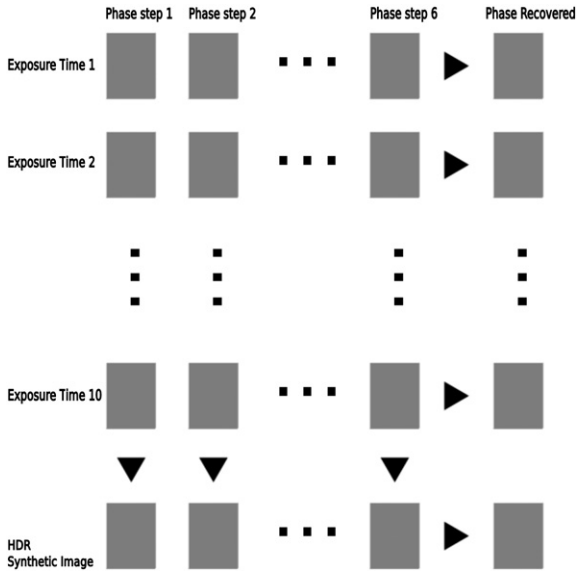

Fig. 5. Rows are exposure times and columns are phase steps. For each exposure time, we have one phase recovered and for each phase step we have one synthetic image (HDR). "Best image" is the set of phase steps and phase recovered at exposure time 1/556 s.

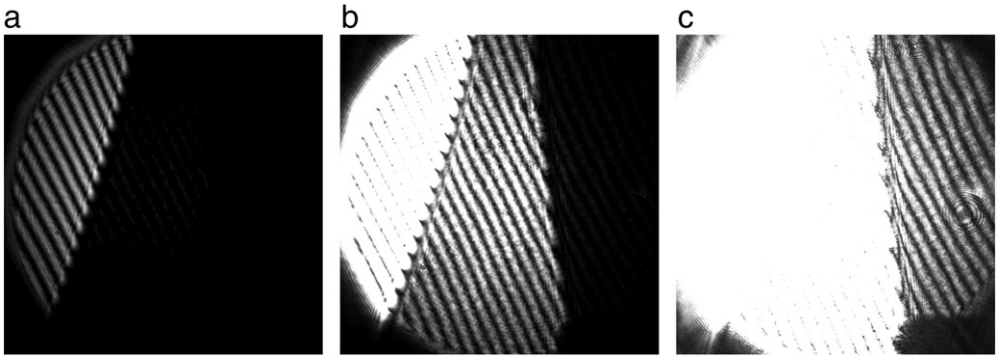

Fig. 6. Interferogram with 3 different exposure times. (a) Interferogram exposure time 1/10,000. (b) Interferogram exposure time 1/556. (c) Interferogram exposure time 1/16.

process, we made a simulation before to apply the methodology to our experimental case.

In Section 2 a simulation is presented to review some concepts to quantify the contrast improvement, which are shown graphically. In Section 3, we applied the mentioned methodology to the experimental data obtained from a set of interferograms acquired in a Mach–Zehnder set-up. The experimental set-up is used for routinely testing the optical quality of a liquid crystal device (LC) under development in our laboratory. We use different polarization areas in the same acquisition to analyze the optical aperture of the device that produces areas with very different illumination levels so that the normalization process is necessary to successfully extract the phase. Finally, conclusions are given in Section 4.

2. Simulation

Using Eq. (4), it is constructed as an interferogram in nine different and relative exposure times. A simulated interferogram with a relative exposure of 0.5 has half of the exposure in respect to the other one with a relative exposure of 1. Fig. 1(a) shows the most under-saturated simulated interferogram which, includes 5% of noise level to incorporate the influence of electronic noise (dark current, photon noise, readout, etc.), characterized by pixel to pixel variation. The noise was performed by Gaussian distribution added in the intensity, being different to each exposure time image. A spatial distribution created to simulate the main effect of the stray-light produced in a typical acquisition process was superposed to the first contribution mentioned. This spatial distribution is also the background simulation. It is composed of a squared cosine distribution and two-dimensional parabolic function. The amplitude modulation is not constant and it is formed by two-dimensional parabolic function. Fig. 1(b) shows the interferogram profile following the line in Fig. 1(a).

Having the simulated set of nine images, the response function was computed as it was explained in Section 1. Then, the HDR interferometric pattern was constructed. Clearly, this response function is not the real one as that of a CCD.

The HDR algorithm basically joins a set of images with different exposure times, and creates only one synthetic image, which has a high dynamic range of the radiance map in the scene [16]. Although, the HDR radiance map carries the information of all areas of the image, it still shows different amplitude levels that do not allow phase recovery. Thus, it is necessary to normalize to take advantage of the digital resolution achieved with the HDR process. In the experimental case (Section 3), the difference of the amplitude levels after applying the HDR process will be clearly explained and illustrated.

The minimal number of images needed to increase the dynamic range is two [13]. Building the HDR image with more than two would allow a better sample of over-saturated and under-saturated areas. To understand that advantage, Fig. 2(a) shows how the root square mean error (*RMSE*) decreases when there are more images to build the HDR image. Theoretically, the curve should be asymptotic, however due to the typical simulation artifacts, an increase in the error when the normalization algorithm is applied after the eighth image is noted. Also it is noted, after a certain number of frames that there is no advantage.

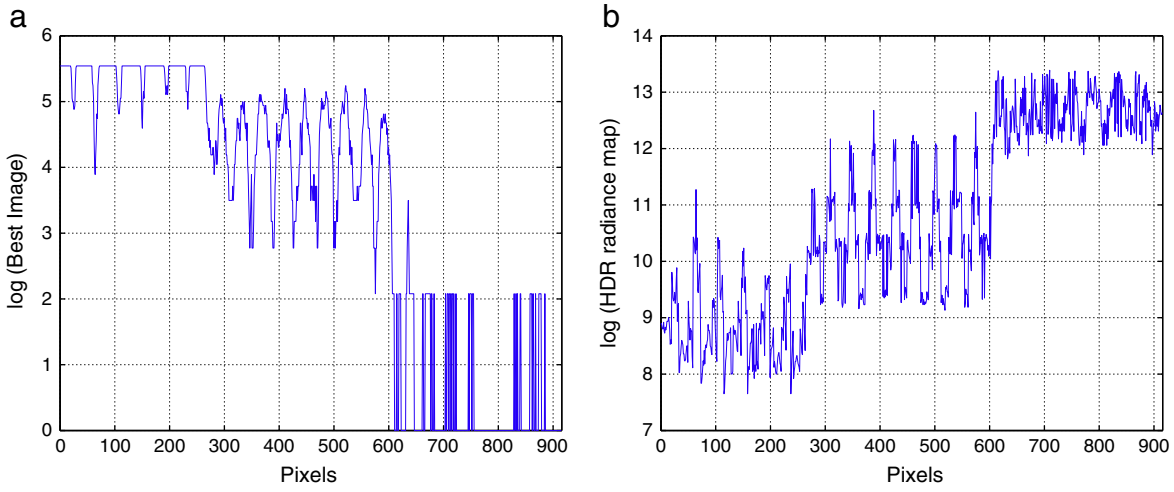

Fig. 7. Improvement of the signal-to-noise applying HDR process. (a) Best image logarithm. (b) HDR radiance map logarithm.

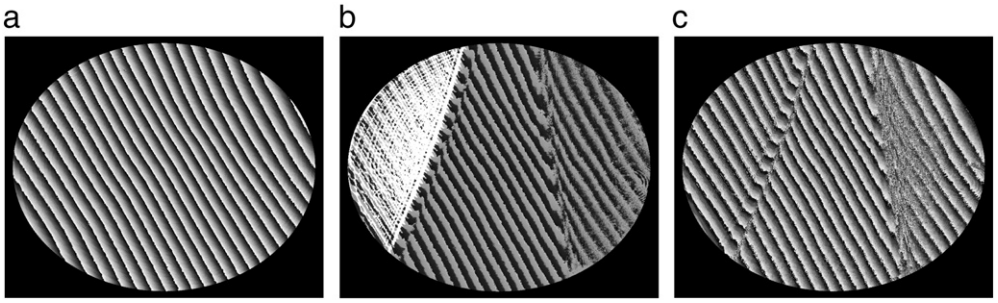

Fig. 8. Phase reconstruction. Phase modulo 2π. (a) Reference image. (b) Best image. (c) HDR.

The *RMSE* is calculated as:

$$RMSE = \sqrt{\frac{\sum_{x=1}^{n}\sum_{y=1}^{m}[I_{WoN}(x,y) - I_{\mathrm{HDR}}(x,y)]^2}{n \times m}}, \quad (9)$$

where $I_{WoN}(x,y)$ is the target (a simulated image without noise and background), $I_{\mathrm{HDR}}(x,y)$ is the synthetic image. In Fig. 2(a), the dotted line, or best-simulated image, is the smallest error compared to the target of the nine simulated images. It is evident that this error is substantially higher than the one of the HDR images, represented by the continuous line.

Fig. 2(a) shows how the error decreases in the absence of pixel-to-pixel noise. Note that when this noise is introduced in Fig. 2(b), the error is amplified.

The final fringe pattern after process (HDR and normalization) with the lower *RMSE* is shown in Fig. 3(a), and its profile in Fig. 3(b). The error reduction achieved is more than 35%. Note in Fig. 3(b), how the background is supressed, the amplitude is normalized and the information in over-saturated and under-saturated is recovered.

3. Experimental

Liquid–crystal variable retarders (LCVRs) are an emergent technology for space-based polarimeters [21,22]. They provide many advantages to both ground- and space-based instrumentations with respect to more traditional modulators, in particular low voltage and power requirements, low mass, low volume and large clear apertures [21,22]. However, they have some characteristics that should be taken into account and, if necessary, addressed during the instrument design. One of the more important properties of any polarization modulator is its homogeneity retardance.

Homogeneity retardance value and the wavefront error are closely related. Mechanical changes that stress the glasses produce changes in the wavefront error. Therefore, in homogeneity retardance, the inhomogeneity becomes more evident in certain polarization states [21,22], and having them in one single shot produces a more efficient measure.

The arrangement used is a Mach–Zehnder interferometer, where P2 and the object beam polarize the reference beam, is propagated through P1 and then through a thermo-vacuum chamber (TVC). Within the thermo-vacuum chamber is placed the LC device, and then both beams are recombined and propagated through a third polarizer (P3), with three polarization states (PA1, PA2, PA3), before getting to the CCD, as shown in Fig. 4. With P1 is selected a determined polarization, with P2 the contrast is maximized, and with P3 are obtained three different polarization states in one single shot.

The monochrome CCD used in this experimental case, has 1280×960 pixels and a pixel size of 4.65 μm. The LC used was nematic, with the following properties: LC MLC-6204-100, Dn = 0.1479 at 525 nm and viscosity of 38 mm^2/s (at 20 °C).

As it was mentioned before, the main objective of HDR technique is to acquire a series of images of the same scene, taken at different exposure times. This is a complicated task in interferometry because different agents can cause changes in the phase of the wavefront to be recovered. Air temperature, differential humidity, vibration of moving parts, and other error sources, can produce instabilities on the acquired fringes. However, it is assumed that there are no changes in the scene, as the error sources are controlled in a clean environment.

Fig. 5 shows the procedure to increase the dynamic range to every phase shift. That means that, for each of the six phase shifts, the interferogram is obtained in ten different exposure times. Therefore, there are six HDR interferogram patterns in different phase shifts, and each one of them are normalized to then recover the phase. The exposure times selected were [1/10,000, 1/5000, 1/3333, 1/1250, 1/556, 1/294, 1/139, 1/65, 1/32, 1/16] s.

In the following the so-called “best image” and “reference image” will be explained to understand what comes after the results. The “best image” is the group of interferograms in the six phase shifts, the phase modulo 2π, the unwrapped phase and the unwrapped

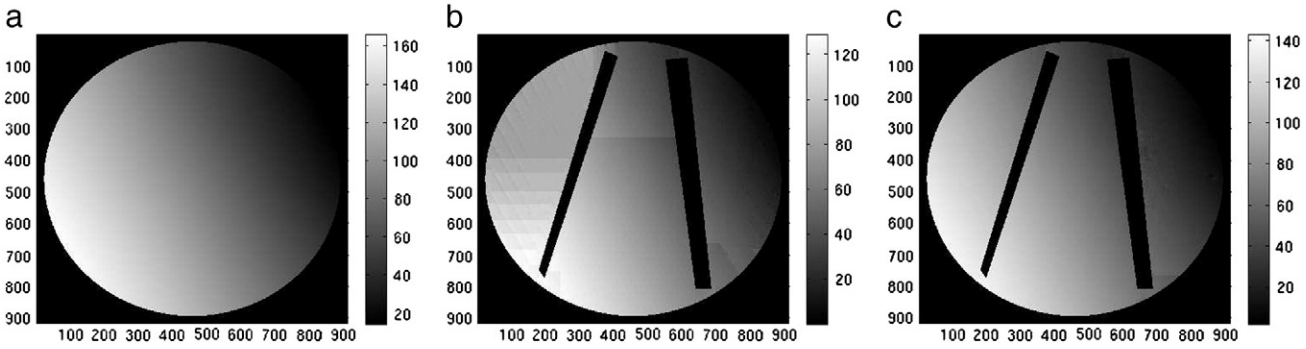

Fig. 9. Phase reconstruction. Phase unwrapped including tilt and piston. (a) Reference image. (b) Best image. (c) HDR.

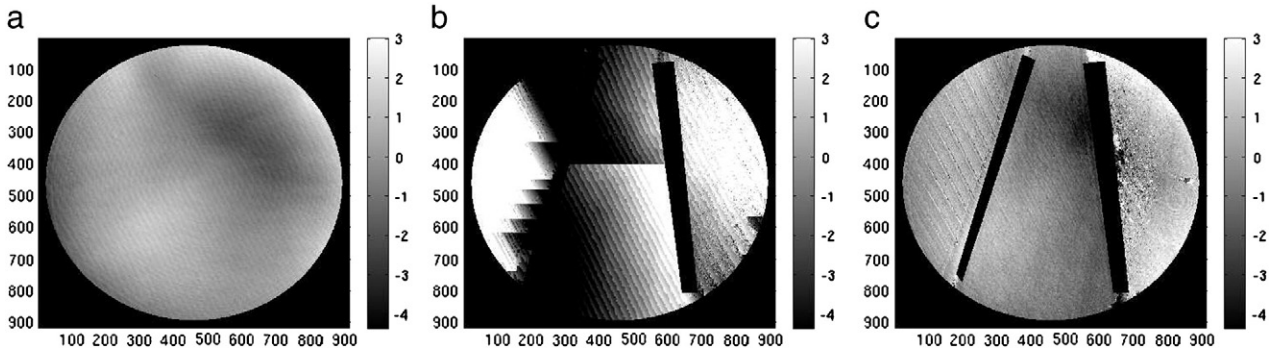

Fig. 10. Phase reconstruction without tilt and piston. (a) Reference image. (b) Best image. (c) HDR.

phase without tilt and piston. The latter one was obtained in the exposure time 1/516 s (see Figs. 6(b), 8(b), 9(b) and 10(b)). The "best image" is called like that because it has the smaller *RMSE* of all exposure times. The *RMSE* was calculated only with the unwrapped phase without tilt and piston using Eq. (9), having as a target the unwrapped phase without tilt and piston, when P3 was removed and LC was deactivated ("reference image"). Therefore, what is called "reference image" is the three images, the phase modulo 2π, the unwrapped phase and the unwrapped phase without tilt and piston (see Figs. 8(a), 9(a) and 10(a)).

Fig. 6 shows an interferogram in three different exposure times. Note the three polarization states and the wide difference between the most over-saturated and the most under-saturated zones. Applying the not normalized HDR method (Fig. 7(b)), it can be proved that the missing information from the over-saturated and under-saturated zones (Fig. 7(a)) is better sampled, and it is possible to recover the information to have it in only one interferogram. The exposure time used in Fig. 7(a) is 1/516 s. In Fig. 7(a) and (b), the data logarithm to appreciate the amplitude difference is shown.

Once the six HDR interferogram patterns are gotten, these are normalized using the procedure explained in Section 1. Although, some algorithms of phase modulo 2π normalized within the process [23,24], they do not suppress the background. For that reason, normalization algorithms are useful as a pre-process, as variations in the background and modulation amplitude, produce error in the phase extraction. The algorithm used in the recovery of the phase modulo 2π is developed by Wang and Han [23].

The algorithm to phase modulo 2π extraction is to establish convergence of least squares quickly and accurately. Data entry for the process is low, only three interferograms in different phase shifts, not necessarily known, are enough to extract the phase. Phase shifts of the estimated inputs do not have to be very accurate. The algorithm has three basic steps, the first one is the iteration pixel by pixel to determine the phase distribution; the second step is the iteration frame by frame where to determine phase shifts as it is assumed that the background intensity and the modulation amplitude do not have a pixel by pixel variation, and there are only changes between frames, and finally the third step, the convergence limit is defined and then steps 1 and 2 are repeated until it is achieved.

Thus, with the procedure explained above the phase modulo 2π is recovered for both the "best image" and the HDR image, and the error is quantified as done in the simulation, taking as "image reference", as explained above. Fig. 8 shows the three phases modulo 2π, and their respective phase unwrapped is shown in Fig. 9, where apparently the phase is recovered in both cases without high error compared with "reference image", but if in the unwrapped phase suppressed tilt and piston contributions are suppressed, the phase in the best image is broken and HDR phase is recovered with low error (see Fig. 10). In HDR image and "best image" polarizer border effect was suppressed. The *RMSE* for best image is 10.6 and the *RMSE* for HDR images is 1.4.

4. Conclusions

We demonstrated that the proposed method is an efficient tool in phase recovering for those cases where the intensity differences in multiple image zones are disproportionate, and that with a single image, phase reconstruction would be not satisfactory and it would have appreciable errors.

This method can also be invaluable in speckle interferometry, especially in the case of studying materials with different reflectances, the presented method would provide a huge benefit in phase recovering.

Finally the proposed method is easy to implement, it does not need additional hardware and neither optical set-up change. It can be used in any interferometric set-up.

Method uses two very well-known tools from different areas of science, one widely used in image processing and the other one in signal treatment and fringe interpretation.

In order to solve the environment problem, where they produce changes in the scene, we propose a solution for the future. It is to acquire in a unique shot the different images using phase shifting techniques. This has been explored in an optical set-up using special light modulators (SLM) that can suppress the mentioned changes that occurred on the different images. In only one shot it is possible to acquire different relative images taken at different exposure times by means of dividing the CCD in quadrants. In order to do that we placed the SLM in a pupil location and it was used as diffraction grating in order to separate angularly the different images.

References

[1] R.M. Groves, G. Pedrini, W. Osten, Applied Optics 47 (2008) 5550.
[2] C. Quan, C.J. Tay, T. Wu, S.H. Wang, H.M. Shang, Optics Communications 237 (2004) 243.
[3] S. Ri, M. Fujigaki, Y. Morimoto, Applied Optics 47 (2008) 5400.
[4] G. Pedrini, H.J. Tiziani, I. Alexeenko, Applied Optics 41 (2002) 648.
[5] J. Vargas, T. Koninckx, J.A. Quiroga, L.V. Gool, Optical Engineering 47 (2008) 053602.
[6] J. Vargas, R. Restrepo, J.A. Quiroga, T. Belenguer, Optics Communications 284 (2011) 4141.
[7] P. Irawan, J.A. Ferwerda, S.R. Marschner, Proc. Eurographics Symposium on Rendering, 2005, p. 231.
[8] L. Wang, L.-Y. Wei, K. Zhou, B. Guo, H.-Y. Shum, Proc. Eurographics Symposium on Rendering, 2007, p. 321, 2007.
[9] M. Uslenghi, M. Fiorini, G. Sarri, Nuclear Instruments & Methods in Physics Research A 518 (2004) 223.
[10] G.C. Holst, CCD Arrays Cameras and Displays, JCD Publishing, Bellingham, WA, 1998.
[11] L. Cerman, V. Hlavac, Proc of the Computer Vision Winter Workshop, 2006, p. 76, 2006.
[12] Y. Tsin, V. Ramesh, T. Kanade, Proc Eighth International Conference on Computer Vision (ICCV), 2001, p. 480, 2001.
[13] P.E. Debevec, J. Malik, Recovering High Dynamic Range Radiance Map from Photographs. *SIGGRAPH97*, 1997, p. 369, 1997.
[14] T. Mitsunaga, S.K. Nayar, Proc Computer Vision and Pattern Recognition (CVPR), 1999, p. 374.
[15] M.D. Grossberg, S.K. Nayar, Proc IV European Conference on Computer Vision, 2002, p. 189, 2002.
[16] E. Reinhard, G. Ward, S. Pattanaik, P.E. Debevec, The Morgan Kaufmann Series in Computer Graphics Morgan Kaufmann, 2005.

[17] J.A. Quiroga, M. Servin, Optics Communications 224 (2003) 221.
[18] J.A. Quiroga, J.A. Gomez-Pedrero, A. Garcia-Botella, Optics Communications 197 (2001) 43.
[19] Q. Yu, K. Andresen, W. Osten, W. Jueptner, Applied Optics 35 (1996) 3783.
[20] M. Servin, J.A. Quiroga, J.L. Marroquin, Journal of the Optical Society of America. A 20 (2003) 925.
[21] R.L. Heredero, N. Uribe-Patarroyo, T. Belenguer, G. Ramos, A. Sánchez, M. Reina, V. Martínez-Pillet, A. Álvarez-Herrero, Applied Optics 46 (2007) 689.
[22] N. Uribe-Patarroyo, A. Alvarez-Herrero, R.L. Heredero, J.C. del Toro Iniesta, A.C. Lopez Jimenez, V. Domingo, J.L. Gasent, L. Jochum, V. Martínez, Physica Status Solidi (c) 5 (2008) 1041.
[23] Z. Wang, B. Han, Optics Letters 29 (2004) 1671.
[24] J. Xu, Q. Xu, L. Chai, Y. Li, H. Wang, Optics Express 18 (2004) 20620.